Probing valence electronic wave-packet dynamics by all x-ray stimulated Raman spectroscopy: A simulation study

Igor V. Schweigert and Shaul Mukamel*
Department of Chemistry, University of California, Irvine, California 92697-2025, USA
(Received 2 May 2007; published 12 July 2007)

The femtosecond impulsive stimulated x-ray Raman signal from quinolinol is simulated and analyzed using the doorway-window representation of pump-probe spectroscopy. A valence electronic wave packet prepared by the pump, tuned on resonance with a given core hole, is localized in the vicinity of a selected atom and probed by a window localized on a different atom, selected by the probe pulse. All valence electronic states within the pulse bandwidths can be observed with high spatial and temporal resolution by monitoring the variation of the signal with the delay between the pulses. Natural orbital representation of the reduced single-electron density matrix is used to visualize the dynamics of the valence wave packet, described as a linear combination of determinants made of occupied and unoccupied Kohn-Sham orbitals.

DOI: 10.1103/PhysRevA.76.012504 PACS number(s): 33.20.Rm, 42.65.Dr

I. INTRODUCTION

X-ray absorption near-edge spectroscopy (XANES) provides a direct, atom-specific probe of unoccupied electronic orbitals [1]. Recent advances in ultrafast x-ray sources have paved the way for time-resolved XANES studies of electronic and structural changes of molecules undergoing chemical reactions [2–7]. The electronic and molecular structure of the transient species in photoinitiated reactions have been studied using 100 ps x-ray pulses [2–4]. Subfemtosecond x-ray pulses have been combined with a few-cycle visible pump to study electronic relaxation in atoms [5] and oscillations of the photoelectron kinetic energy [6]. Other possible schemes such as infrared–x-ray pump-probe [8], optical–x-ray sum frequency generation [9], and coherent x-ray Raman scattering [10] were studied theoretically.

In this work, we simulate an all x-ray pump-probe experiment, whereby the interaction with an attosecond x-ray pump tuned resonantly to a specific core hole transition creates an electronic wave packet, which is then detected by a delayed x-ray probe. The dependence of the probe absorption on the delay provides information on the time evolution of the valence electronic states constituting the wave packet. Due to localization of the core shell, the created valence wave packet is initially centered on the atom whose core shell is resonant with the pump frequency. Similarly, the probe absorption reflects the unoccupied states in the vicinity of the core-shell resonant with the probe frequency. By tuning the pump and the probe frequencies, one can choose where the wave packet is created and where it is probed. Tuning the pump and the probe frequencies to different core transitions makes it possible to study the delocalization of the electronic states.

Resonant interaction with the pump x-ray field results in multiple excitation and deexcitation events of the core electrons. These are accompanied by valence excitations, similarly to how vibrational states are excited in the optical Raman process. This technique is thus the x-ray analogue of impulsive Raman scattering in the visible. In the latter case, the pump is coupled to a valence (rather than a core) state and prepares a vibrational wave packet. The x-ray technique offers a higher (attosecond) time resolution and a bird's eye view of many valence electronic excitations. This is complimentary to resonant optical spectroscopy which looks at one state at a time and often has strict selection rules limiting the accessible states.

Pump-probe spectroscopy is the simplest nonlinear optical technique. The signal, defined as the difference in the absorption of the probe, with and without the pump, has generally three contributions: Ground-state bleaching (GSB), stimulated emission (SE), and excited-state absorption (ESA) [11]. In the SE and ESA, the molecule is prepared by the pump in the core excited state. The GSB is a Raman-type contribution whereby two interactions with the pump create a valence electron wave packet (no core hole), which includes multiple valence electronic states covered by the pulse bandwidths. The lifetime of the core excited states contributing to the SE and ESA ($\sim$10 femtosecond for first-row atoms) is much shorter than the lifetime of valence excited states (typically longer than 1 ps). The GSB signal thus offers a much longer time window for observation, since it is not limited by the core hole lifetime. We shall focus on the GSB contribution to the pump-probe signal observed for delays longer than 10 femtosecond. This technique is also known as stimulated Raman. A related coherent x-ray Raman four pulse experiment was proposed in Ref. [10] and simulated using a tight binding model.

In Sec. II, the sum-over-states expression for the pump-probe signal is derived using the nonlinear response function [12]. The expression is recast in the doorway-window representation [13], whereby the signal is written as the Liouville-space overlap between a doorway operator representing the electronic wave packet created by the pump and a window operator representing the interaction with the probe. This representation provides an intuitive picture of the pump-probe measurement by dividing it into wave packet creation, propagation, and detection stages.

The computational algorithm is outlined in Sec. III. The core-excited states are described by the valence excited states

*smukamel@uci.edu

of the equivalent-core (or, $Z+1$) molecule [14]. The valence states of the original and equivalent-core molecules are represented by determinants made of the ground-state Kohn-Sham orbitals. Expressions for the necessary transition frequencies and dipole moments are given elsewhere [15].

In Sec. IV, we define the reduced one-electron doorway and window operators that provide a real-space picture for the corresponding wave packets. Within the single-determinant approximation, the reduced operators are given by sums over occupied-unoccupied molecular orbital pairs. The reduced operators are then recast in a compact form using the natural-orbital representation. Natural orbitals provide a compact and intuitively simple description of the one-electron reduced density matrices [16]. The concept has recently been extended to transition density matrices [17]. The reduced doorway and window operators can be similarly represented by a sum over particle-hole natural orbital pairs. Unlike the molecular-orbital representation, where many pairs contribute, only a few natural-orbital pairs dominate the reduced operators. Displaying the doorway natural orbitals as a function of the delay provides a real-space picture for the evolution of the density matrix after the pump. The probe absorption signal is given by the projection of the doorway orbitals on the window orbitals.

In Sec. V we present simulations of the N and O K-edge signals of 5-quinolinol, a two-ring system in which the O and N atoms are located on different rings. The stimulated Raman signal for delays varying from 20 to 100 femtoseconds was simulated for the N $1s$ pump–N $1s$ probe and N $1s$ pump–O $1s$ probe pulse configurations. The evolution of the density matrix for delays from 80 to 81 femtosecond is displayed using the snapshots of the doorway natural orbitals. The relation between the N $1s$/N $1s$ and N $1s$/O $1s$ signals and localization of the valence wave packet is demonstrated. Our results are summarized in Sec. VI.

II. DOORWAY-WINDOW REPRESENTATION OF THE PUMP-PROBE SIGNAL

We consider a pump-probe experiment carried out with two x-ray pulses. The electric field is given by

$$E(\boldsymbol{r},t) = \mathcal{E}_1(t)e^{i\boldsymbol{k}_1\boldsymbol{r}-i\omega_1 t} + \mathcal{E}_1^*(t)e^{-i\boldsymbol{k}_1\boldsymbol{r}+i\omega_1 t} + \mathcal{E}_2(t-\tau)e^{i\boldsymbol{k}_2\boldsymbol{r}-i\omega_2 t} + \mathcal{E}_2^*(t-\tau)e^{-i\boldsymbol{k}_2\boldsymbol{r}+i\omega_2 t}. \quad (1)$$

Here, $\mathcal{E}_1(t)$, $\boldsymbol{k}_1$, and ω_1 are, respectively, the temporal envelope, the wave vector, and the carrier frequency of the pump and $\mathcal{E}_2(t)$, $\boldsymbol{k}_2$, ω_2 are those of the probe. τ is the delay between the two pulses. The time-integrated pump-probe signal, defined as the difference in the probe absorption with and without the pump pulse, is given by

$$S(\omega_1,\omega_2,\tau) = -\,\mathrm{Im}\int_{-\infty}^{\infty} dt\, \mathcal{E}_2^*(t)P^{(3)}(\boldsymbol{k}_2,t), \quad (2)$$

where $P^{(3)}$ is the polarization induced in the molecule by interaction with the pulses to third order in the matter-field interaction (second order in the pump and first order in the probe field) [12]. We consider sequential measurements

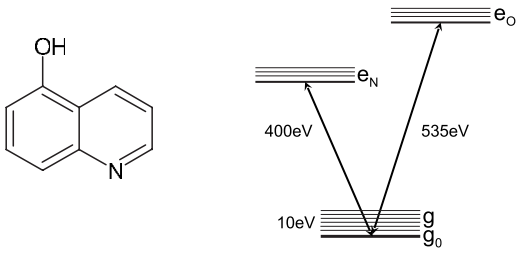

FIG. 1. Left panel: Molecular structure of 5-quinolinol. Right panel: Valence and core-excited states contributing to the stimulated Raman signal. g denotes valence states with no core electron excited (including the ground state g_0) and e_N (e_O) denotes states with N $1s$ (O $1s$) core electron excited.

where the pump-probe delay τ (10–100 femtosecond) is much longer than the pulses' durations ($\leqslant$1 femtosecond). Assuming the dipole interaction $\hat{H}_{\mathrm{int}}=-\hat{V}E(\boldsymbol{r},t)$, the signal is given by

$$\begin{aligned} S(\omega_1,\omega_2,\tau) &= \mathrm{Im}\int_{-\infty}^{\infty} dt \int_0^{\infty} dt_3 \int_0^{\infty} dt_2 \int_0^{\infty} dt_1 R^{(3)}(t_3,t_2,t_1) \\ &\times [\mathcal{E}_2^*(t-\tau)\mathcal{E}_2(t-t_3-\tau)\mathcal{E}_1(t-t_3-t_2)\mathcal{E}_1^*(t-t_3-t_2-t_1) \\ &\times e^{i\omega_2 t_3 - i\omega_1 t_1} + \mathcal{E}_2^*(t-\tau)\mathcal{E}_2(t-t_3-\tau)\mathcal{E}_1^*(t-t_3-t_2) \\ &\times \mathcal{E}_1(t-t_3-t_2-t_1)e^{i\omega_2 t_3 + i\omega_1 t_1}]. \end{aligned} \quad (3)$$

The third-order response function $R^{(3)}$ is given in terms of four-point correlation functions of the dipole operator [12].

The process can be separated into three steps: (i) two interactions with the pump create a coherent excited-state density matrix wave packet; (ii) during τ, the wave packet propagates freely; (iii) the final state of the wave packet affects the probe absorption resulting in the pump-probe signal [13]. The signal is recast in the doorway-window representation (Appendix A),

$$S(\omega_2,\omega_1,\tau) = \mathrm{Re}\langle\langle W(\omega_2)|D(\omega_1,\tau)\rangle\rangle. \quad (4)$$

Here, the doorway operator $\hat{D}(\omega_1,\tau)$ represents the electronic density matrix that arises due to two interactions with the pump, while the window operator represents the states that contribute to the probe absorption. In particular, the probe absorption in the absence of the pump is given by $\langle\langle W(\omega_2)||\rho_0\rangle\rangle$, where ρ_0 is the ground-state density matrix. Closed expressions for $\hat{D}$ and $\hat{W}$ [Eqs. (A6) and (A7), respectively] are obtained by expanding the field-free molecular Green's function in electronic eigenstates

$$\hat{G}(t) = \sum_{\nu_1\nu_2} |\Psi_{\nu_1}\rangle\langle\Psi_{\nu_2}| e^{-i\omega_{\nu_1\nu_2}t-\Gamma_{\nu_1\nu_2}t}, \quad (5)$$

where $\omega_{\nu_1\nu_2}\equiv E_{\nu_1}-E_{\nu_2}$ is the frequency and $\Gamma_{\nu_1\nu_2}$ is the dephasing rate of the transition between states Ψ_{ν_1} and Ψ_{ν_2}.

In what follows, we consider resonant N and O K-edge measurements in 5-quinlinol (Fig. 1). The bandwidth of a 600-attosecond pulse duration ($\sim$6 eV) is much smaller than

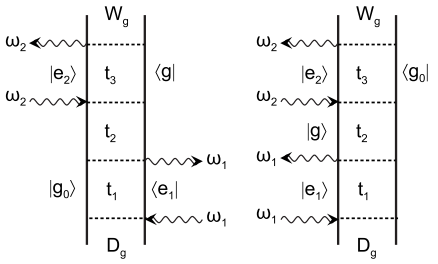

FIG. 2. Two GSB Liouville-space pathways contributing to the stimulated Raman signal.

the splitting of the N and O K-edges ($\sim$100 eV). Correspondingly, only coherences between valence (no core hole) states and coherences between single core-excited (one core hole) states contribute to the signal, which is given by a sum of six Liouville-space pathways (see Ref. [11] and Appendix A).

We shall consider pump-probe delays longer than the core hole lifetime determined by the Auger decay. The molecules prepared by the pump in the coherences between the core-excited states are ionized and their core transitions are off-resonant with the probe frequency. The signal is then dominated by the GSB contribution (Fig. 2)

$$S(\omega_2,\omega_1,\tau) = \mathrm{Re}\ \mathrm{Tr}[W_g^\dagger D_g(\tau)], \tag{6}$$

where

$$\hat{D}_g(\tau) = \sum_g \sum_g |\Psi_g\rangle\langle\Psi_{g_0}| D_g(\omega_1) e^{-i\omega_{gg_0}\tau} + \mathrm{H.c.}, \tag{7}$$

$$D_g(\omega_1) = \sum_{e_1} V_{ge_1} V_{e_1g_0} \mathcal{I}_1(\omega_{gg_0}, \omega_1 - \omega_{e_1g_0}), \tag{8}$$

$$\hat{W}_g^\dagger = \sum_g |\Psi_{g_0}\rangle\langle\Psi_g| W_g(\omega_2) + \mathrm{H.c.}, \tag{9}$$

$$W_g(\omega_2) = \sum_{e_2} V_{g_0e_2} V_{e_2g} \mathcal{I}_2(-\omega_{gg_0}, \omega_2 - \omega_{e_2g}), \tag{10}$$

and

$$\mathcal{I}_j(\Omega_2,\Omega_1) = \int_{-\infty}^{\infty} dt_2 \int_0^{\infty} dt_1 \mathcal{E}_j^*(t_2)\mathcal{E}_j(t_2-t_1) e^{i\Omega_2 t_2 + i\Omega_1 t_1} \tag{11}$$

represents the pump and probe envelopes.

The stimulated Raman signal is finally given by

$$S(\omega_2,\omega_1,\tau) = 2\ \mathrm{Re} \sum_{g,e_1,e_2} V_{g_0e_2} V_{e_2g} V_{ge_1} V_{e_1g_0} e^{-i\omega_{gg_0}\tau} \times \mathcal{I}_2(-\omega_{gg_0}, \omega_2 - \omega_{e_2g}) \mathcal{I}_1(\omega_{gg_0}, \omega_1 - \omega_{e_1g_0}). \tag{12}$$

Since the contribution of the ground state Ψ_{g_0} to the signal is independent of τ, we shall separate it from the contribution of valence excited states and define the valence operators

$$\hat{D}_v(\tau) = \sum_{g\neq g_0} |\Psi_g\rangle\langle\Psi_{g_0}| D_g e^{-i\omega_{gg_0}\tau} + \mathrm{H.c.}, \tag{13}$$

$$\hat{W}_v^\dagger = \sum_{g\neq g_0} |\Psi_{g_0}\rangle\langle\Psi_g| W_g + \mathrm{H.c.} \tag{14}$$

The stimulated Raman signal with the τ-independent component removed is finally given by

$$\bar{S}(\omega_2,\omega_1,\tau) = \mathrm{Re}\ \mathrm{Tr}[\hat{W}_v^\dagger \hat{D}_v]. \tag{15}$$

III. VALENCE AND CORE EXCITED STATES VIA KOHN-SHAM DETERMINANTS IN THE EQUIVALENT-CORE APPROXIMATION

The stimulated Raman signal [Eq. (12)] depends on the transition frequencies and dipole moments between valence and core-excited states. In order to evaluate these quantities using standard *ab initio* codes, we rely on the equivalent-core approximation, whereby the core excitations are described by the valence excitations of the equivalent-core molecule. The latter have an extra valence electron and the charge of the nucleus whose core shell is in resonance is incremented by one. We further use determinants made of ground-state Kohn-Sham orbitals to represent the ground and excited states of the original and equivalent-core molecules

$$\Psi_g = \hat{\mathcal{A}}_N \phi_1(\boldsymbol{r}_1) \ldots \phi_p(\boldsymbol{r}_q) \ldots \phi_N(\boldsymbol{r}_N), \tag{16}$$

$$\Psi_e = \hat{\mathcal{A}}_{N+1} \tilde{\phi}_1(\boldsymbol{r}_1) \ldots \tilde{\phi}_r(\boldsymbol{r}_s) \ldots \tilde{\phi}_{N+1}(\boldsymbol{r}_{N+1}), \tag{17}$$

$$\omega_{gg_0} = \epsilon_p - \epsilon_q, \tag{18}$$

$$\omega_{eg} = \omega_e + \tilde{\epsilon}_r - \tilde{\epsilon}_s - \epsilon_p + \epsilon_q. \tag{19}$$

Here, ϕ_n and ϵ_n are the Kohn-Sham orbitals and orbital energies of the original molecule, $\tilde{\phi}_n$ and $\tilde{\epsilon}_n$ are those of the equivalent-core molecule. $\hat{\mathcal{A}}_N$ denotes an antisymmetric sum over $N!$ possible permutations of two electron indices. In Eq. (16), the ground-state KS determinant ($p=q$) corresponds to the ground state, and the singly-substituted determinants ($p>N$, $q\leqslant N$) to the valence excited states. Similarly, in Eq. (17), the ground-state determinant ($r=s$) corresponds to the lowest core-excited state, and the singly substituted determinants ($r>N+1$, $s\leqslant N+1$) to the remaining core-excited states. ω_e is adjusted to fit the frequency of the lowest peak in the simulated XANES to experiment. The transition dipole moments between the valence and core-excited states are calculated using the protocol described in detail in Ref. [15].

IV. NATURAL-ORBITAL REPRESENTATION OF THE REDUCED ONE-ELECTRON DOORWAY AND WINDOW OPERATORS

Operator $\hat{D}_v(\tau)$ describes the evolution of the many-electron density matrix during the delay between the pump and the probe pulses. It depends on $2N$ coordinates (where N

is the number of electrons), thus providing no means for visualizing this evolution. In order to obtain a real-space representation of the electronic wave packet described by $\hat{D}_v(\tau)$, we define the reduced one-electron doorway operator

$$D_v(\boldsymbol{r},\boldsymbol{r}',\tau) = \sum_{g\neq g_0} D_g(\omega_1)e^{-i\omega_{gg_0}\tau}\int d\boldsymbol{r}_2 \ldots d\boldsymbol{r}_N \times \Psi_g(\boldsymbol{r},\boldsymbol{r}_2,\ldots,\boldsymbol{r}_N)\Psi^*_{g_0}(\boldsymbol{r}',\boldsymbol{r}_2,\ldots,\boldsymbol{r}_N) \quad (20)$$

and, similarly, the reduced window operator

$$W_v(\boldsymbol{r},\boldsymbol{r}') = \sum_{g\neq g_0}\int d\boldsymbol{r}_2 \ldots d\boldsymbol{r}_N \Psi_{g_0}(\boldsymbol{r},\boldsymbol{r}_2,\ldots,\boldsymbol{r}_N) \times \Psi^*_g(\boldsymbol{r}',\boldsymbol{r}_2,\ldots,\boldsymbol{r}_N). \quad (21)$$

In terms of the reduced operators, the stimulated Raman signal [Eq. (15)] can be recast in the form of the real-space overlap between the doorway and window wave packets

$$\bar{S}(\omega_2,\omega_1,\tau) = 2\,\mathrm{Re}\,\mathrm{Tr}\int d\boldsymbol{r}\,d\boldsymbol{r}' D_v(\boldsymbol{r},\boldsymbol{r}',\tau)W_v(\boldsymbol{r}',\boldsymbol{r}). \quad (22)$$

Thus the real-time, real-space evolution of the pump-induced density matrix wave packet is given by $D_v(\boldsymbol{r},\boldsymbol{r}',\tau)$ and the stimulated Raman signal is given by its projection onto the window wave packet $W_v(\boldsymbol{r}',\boldsymbol{r})$.

Within the single-determinant approximation [Eq. (16)], Eqs. (20)–(22) reduce to

$$D_v(\boldsymbol{r},\boldsymbol{r}',\tau) = \sum_i^{\text{occ.}}\sum_a^{\text{unocc.}} d_{ia}e^{-i(\epsilon_a-\epsilon_i)\tau}\phi_a(\boldsymbol{r})\phi^*_i(\boldsymbol{r}') + \text{c.c.}, \quad (23)$$

$$W_v(\boldsymbol{r},\boldsymbol{r}') = \sum_i^{\text{occ.}}\sum_a^{\text{unocc.}} w_{ia}\phi_i(\boldsymbol{r})\phi^*_a(\boldsymbol{r}') + \text{c.c.}, \quad (24)$$

and

$$\bar{S}(\omega_2,\omega_1,\tau) = 2\,\mathrm{Re}\sum_i^{\text{occ.}}\sum_a^{\text{unocc.}} w_{ia}d_{ia}e^{-i\omega_{gg_0}\tau}. \quad (25)$$

Note that if only the excitations of the pure one-electron character contribute to the doorway and window operators, then the reduced doorway operator will carry the same amount of information as the many-electron density matrix. This is not the case, in general, if the valence states contain two-electron-type excitations. Indeed, if the many-body expansions for the ground Ψ_{g_0} and a valence excited state Ψ_g differ by a doubly-substituted determinant, their contribution to the reduced doorway operator vanishes. Such excitations are not included in Eq. (16), and Eqs. (15), (22), and (22) are equivalent within the present approximation for excited states.

The reduced doorway operator can be visualized by displaying the pairs of the occupied and unoccupied molecular orbitals contributing to Eq. (23). However, in the case N and O 1*s* signals of quinolinol, a large number of pairs contribute to the sum with equally significant weights. The natural-orbital basis (i.e., the basis in which the doorway operator is diagonal) may offer a more compact representation for this operator. In this representation (Appendix B), the doorway operator is given by a sum over the hole-particle natural-orbital pairs

$$D_v(\boldsymbol{r},\boldsymbol{r}',\tau) = \sum_\xi d_\xi(\tau)\phi^p_\xi(\boldsymbol{r},\tau)\phi^{h*}_\xi(\boldsymbol{r}',\tau) + \text{c.c.}, \quad (26)$$

where ϕ^p_ξ represent the doorway particle and ϕ^h_ξ represent doorway hole natural orbitals.

Similarly, for the window operator we have

$$W_v(\boldsymbol{r},\boldsymbol{r}') = \sum_\xi w_\xi\psi^h_\xi(\boldsymbol{r})\psi^{p*}_\xi(\boldsymbol{r}') + \text{c.c.} \quad (27)$$

and Eq. (22) becomes

$$\bar{S}(\omega_2,\omega_1,\tau) = 2\,\mathrm{Re}\sum_{\xi,\xi'} w_{\xi'}d_\xi(\tau)(\psi^p_{\xi'}|\phi^p_\xi(\tau))(\phi^h_\xi(\tau)|\psi^h_{\xi'}). \quad (28)$$

Thus the stimulated Raman signal at delay τ is given by the product of the overlap between the particle doorway and window natural orbitals, overlap between the hole orbitals, and the corresponding weights. Note that unlike the molecular-orbital representation, whereby the weights d_{ia}, w_{ia} and energy differences $\epsilon_a-\epsilon_i$ can be used to calculate the signal for every delay [Eq. (23)], the natural orbitals must be recalculated for each value of the delay.

V. STIMULATED RAMAN SIGNAL OF QUINOLINOL

We have computed the N and O 1*s* signals of quinolinol using the combination of the Becke three-parameter Lee-Yang-Parr (B3LYP) exchange-correlation functional [18] and 6-311G** Gaussian-type basis set [19] to obtain the Kohn-Sham orbitals for the original and the equivalent-core molecules. Figure 3 shows the simulated N 1*s* and O 1*s* XANES of quinolinol. Since experimental spectra of quinolinol were not available, we used the experimental N 1*s* XANES of pyridine [20] and O 1*s* XANES of phenol [21] for the comparison. The simulated N 1*s* XANES of quinolinol features a strong peak at 399.1 eV and two weaker peaks at 403.1 and 404.4 eV, resembling the experimental N 1*s* XANES of pyridine with a dominant peak at 399.1 and a weaker peak at 403.1 eV. The simulated O 1*s* XANES consists of four peaks at 534.9, 537.0, 538.1, and 539.2 eV, in comparison to the three peaks in the experimental O 1*s* XANES of phenol at 534.9, 537.2, and 539.4 eV. We conclude that the present approximation for the core-excited states qualitatively reproduces the relative intensities of the N 1*s* and O 1*s* transitions in quinolinol.

Figure 4 shows the stimulated Raman signal for N 1*s*/N 1*s* ($\omega_1=\omega_2=\omega_N$) and N 1*s*/O 1*s* ($\omega_1=\omega_N$, $\omega_2=\omega_O$) pulse configurations. $\mathcal{I}(\Omega_2,\Omega_1)$ [Eq. (11)] of a Gaussian pulse with 600 attosecond FWHM decays with increasing Ω_1 and Ω_2 and does not exceed 10% of its maximum value for $|\Omega_1|$, $|\Omega_2\pm\Omega_1|>6$ eV. In the simulation, we included the contributions of all states within this window with the same

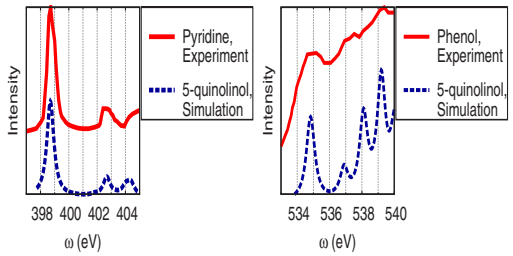

FIG. 3. (Color online) Left panel: Experimental N 1*s* XANES of pyridine [20] and simulated N 1*s* XANES of quinolinol. Right panel: Experimental O 1*s* XANES of phenol [21] and simulated O 1*s* XANES of quinolinol. Lorentzian broadening of 0.3 eV was used in the simulation.

weights and neglected the states outside the window [i.e., $\mathcal{I}(\Omega_2,\Omega_1)$ was taken to be 1 for $|\Omega_1|$, $|\Omega_2 \pm \Omega_1| \leqslant 6$ eV and 0 otherwise]. Also, the imaginary part of $\mathcal{I}(\Omega_2,\Omega_1)$ is much smaller than the real part and was neglected. The stimulated Raman signal [Eq. (15)] is then given by

$$\bar{S}(\omega_2,\omega_1,\tau) = 2\sum_{g\neq g_0} D_g(\omega_1)W_g(\omega_2)\cos(\omega_{gg_0}\tau). \qquad (29)$$

The reduced N 1*s* doorway and window operators $[W_g(\omega_N) = D_g(\omega_N)]$ are dominated by nine valence states and the O 1*s* window operator is dominated by ten. The corresponding occupied-unoccupied molecular orbitals pairs are given in Tables I and II, respectively. The contribution of each state can be identified from the Fourier transform (FT) of the stimulated Raman signal. For the N 1*s*/N 1*s* signal (upper panel of Fig. 5), the intensity of the FT at ω_{gg_0} is proportional to $D_g^2(\omega_N)$. For the N 1*s*/O 1*s* signal (lower panel of Fig. 5), the intensity of the FT at ω_{gg_0} is proportional to $W_g(\omega_O)D_g(\omega_N)$. For states contributing to both signals (such as states at 4.6 and 5.5 eV), one can recover the absolute values of $D_g(\omega_N)$ and $W_g(\omega_O)$ from the intensities of the corresponding peak in the FTs of the N 1*s*/N 1*s* and N 1*s*/O 1*s* signals.

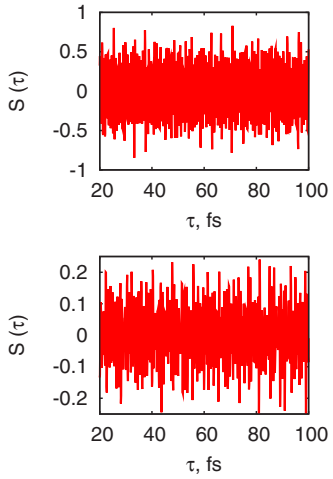

FIG. 4. (Color online) N 1*s*/N 1*s* (upper panel) and N 1*s*/O 1*s* (lower panel) stimulated Raman signal of quinolinol [Eq. (12)].

TABLE I. Molecular-orbital and natural-orbital representation of the reduced N 1*s* doorway operator. Shown are the occupied-unoccupied molecular orbital pairs with $d_{ia} \geqslant 0.2$. At $\tau=0$, these pairs constitute two natural-orbital pairs $\xi=1$ and $\xi=2$ with weights 0.9 and 0.3, respectively.

$\epsilon_a-\epsilon_i$	d_{ia}	i	a	ξ	$d_\xi(0)$
4.6	−0.3	HOMO	LUMO	1	0.9
5.5	0.7	HOMO-1	LUMO	1	0.9
7.7	0.3	HOMO-1	LUMO+3	1	0.9
8.3	−0.2	HOMO	LUMO+6	1	0.9
8.5	−0.2	HOMO-1	LUMO+4	1	0.9
8.8	−0.2	HOMO-3	LUMO+3	2	0.3
9.3	0.3	HOMO-1	LUMO+6	1	0.9
9.6	0.2	HOMO-3	LUMO+4	2	0.3
10.4	−0.2	HOMO-3	LUMO+6	2	0.3

Visualizing the N 1*s* doorway and O 1*s* window operators in real space requires plotting nine and ten molecular orbital pairs, respectively. Natural orbitals provide a much more compact representation of these operators as only two natural-orbital pairs contribute significantly to the N 1*s* doorway and the O 1*s* window operators (Tables I and II). These are displayed in Figs. 6 and 7, respectively. These provide a simple, real-space picture of the interaction with the pump and probe. The interaction with the pump tuned to the N 1*s* transitions creates a superposition of two particle-hole pairs, which contribute with weights 0.9 and 0.3, respectively. The interaction with the probe tuned to the O 1*s* transitions annihilates two particle-hole pairs, with weights 0.8 and 0.5, respectively.

Displaying these pairs for various values of the delay provides real-time snapshots of the wave-packet propagation and explains the signal dependence on the delay. Figure 8 shows the N 1*s*/N 1*s* and N 1*s*/O 1*s* stimulated Raman signals for delays varying between 80 and 81 femtoseconds. Since the N 1*s* window operator is mostly localized to the

TABLE II. Molecular-orbital and natural-orbital representation of the reduced O 1*s* window operator. Shown are the occupied-unoccupied molecular orbital pairs with $w_{ia} \geqslant 0.2$. These pairs constitute two window natural-orbital pairs $\xi'=1$ and $\xi'=2$ with weights 0.8 and 0.5, respectively.

$\epsilon_a-\epsilon_i$	w_{ia}	i	a	ξ'	$w_{\xi'}$
4.6	0.4	HOMO	LUMO	1	−0.8
6.7	−0.4	HOMO	LUMO+3	1	−0.8
8.3	−0.2	HOMO	LUMO+6	2	−0.5
8.8	0.2	HOMO	LUMP+8	2	−0.5
9.6	0.3	HOMO-3	LUMO+4	2	−0.5
10.7	−0.2	HOMO-3	LUMO+5	1	−0.8
10.9	0.3	HOMO-3	LUMO+8	2	−0.5
11.4	−0.4	HOMO	LUMO+12	2	−0.5
11.5	0.2	HOMO-3	LUMO+9	1	−0.8
11.7	−0.3	HOMO-3	LUMO+10	2	−0.5

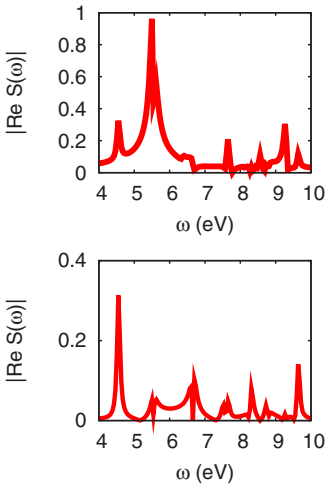

FIG. 5. (Color online) Fourier transform of the N $1s$/N $1s$ (upper panel) and N $1s$/O $1s$ (lower panel) stimulated Raman signal.

ring with N atom, a strong N $1s$/N $1s$ stimulated Raman signal at a given delay indicates the presence of the valence wave packet on that ring. Similarly, a strong N $1s$/O $1s$ signal indicates the presence of the wave packet on the O-ring. Thus the variation of the signal with the delay reflects the propagation of the wave packet through the molecule. This real-time, real-space propagation can be visualized by displaying the doorway natural orbitals. Figure 9 shows the evolution of the doorway pairs between 80 and 81 femtoseconds. The contribution of each pair is determined by its weight, and the overlap with the window hole and particle orbitals [Eq. (28)]. For these delays, the contribution of the first N $1s$ window pair dominates (upper panel of Fig. 9) the N $1s$/N $1s$ signal. The corresponding particle orbital is confined to the ring containing the N atom; hence a strong N $1s$/N $1s$ signal indicates the localization of the wave packet on that ring. Similarly, the contribution of the first O $1s$ window pair (upper panel of Fig. 7) dominates the N $1s$/O $1s$ signal. Since the corresponding window particle orbital is confined to the ring containing the O atom, a strong N $1s$/O $1s$ signal indicates the localization of the wave packet to the O ring. Indeed, at 80.0, 80.25, and 80.5 fs, the first doorway particle orbital is localized to the N ring (Fig. 6) and its contribution to the N $1s$/N $1s$ signal is strong,

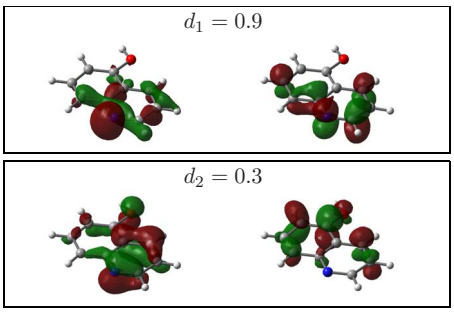

FIG. 6. (Color online) Natural-orbital representations of the N $1s$ doorway operator at τ=0. Shown are the two hole-particle pairs with dominant weights.

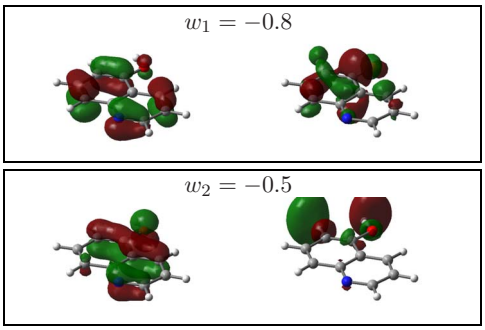

FIG. 7. (Color online) Natural-orbital representations of the O $1s$ window operator. Shown are the two pairs with dominant weights.

while the contribution to the N $1s$/O $1s$ signal vanishes. Alternatively, at 80.0, 80.25, and 80.5 fs, the second doorway particle orbital is localized to the O ring (Fig. 6) and its contribution to the N $1s$/N $1s$ signal is weak and to the N $1s$/O $1s$ is strong. At 80.75 fs, the first doorway particle is localized on the O ring and contributes to the N $1s$/O $1s$ signal, while the second doorway particle is localized on the N ring and contributes to the N $1s$/N $1s$ signal. At 81 fs both particles are delocalized over the two rings and contribute to both the N $1s$/N $1s$ and N $1s$/O $1s$ signal.

VI. CONCLUSIONS

The proposed x-ray stimulated Raman technique should offer a novel probe of the valence excited states in molecules. The signal is obtained from an all-x-ray pump-probe measurement with delays longer than the core-hole lifetime. The interaction with an attosecond pump pulse creates multiple coherences between the valence and core excited states. The contribution of core-excited states rapidly (~10 fs) at-

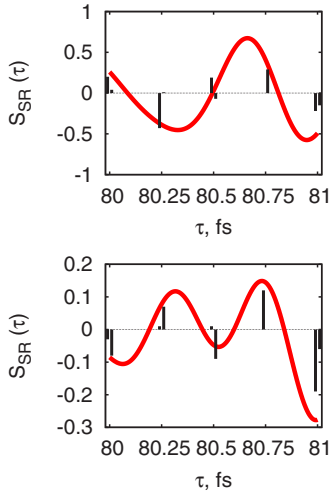

FIG. 8. (Color online) N $1s$/N $1s$ (upper panel) and N $1s$/O $1s$ (lower panel) stimulated Raman signals [Eq. (12)] of quinolinol for delays varying between 80 and 81 fs. Vertical bars show the contributions of the first and the second doorway natural-orbital pairs.

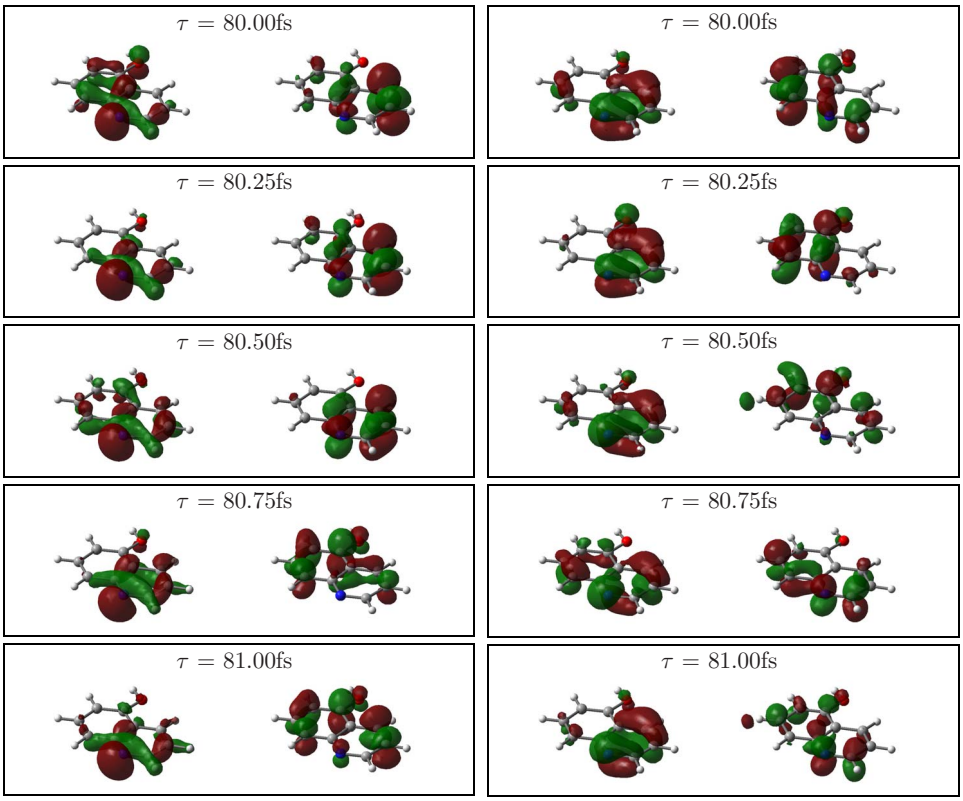

FIG. 9. (Color online) Evolution of the $\xi=1$ (left panel) and $\xi=2$ (right panel) doorway natural-orbital pairs for delays $80 \leqslant \tau \leqslant 81$ fs.

tenuates due to the Auger decay and only valence states contribute to the probe absorption for longer delays. The Raman signal thus reflects the evolution of the valence wave packet, providing information about the temporal and spatial characteristics of the valence excited states.

We have calculated the N 1*s* and O 1*s* stimulated Raman signals of quinolinol using sum-over-states expressions. The necessary valence to core-excited transition frequencies and dipole moments were calculated from first principles, using determinants made of the ground-state Kohn-Sham orbitals within the equivalent-core approximation. The signal was recast in the doorway-window representation, which relates it to the real-time evolution of the valence wave packet. The signal is given by the projection of the wave packet at a given delay (represented by the doorway operator) onto the states contributing to the probe absorption (represented by the window operator). The many-electron doorway and window operators were displayed using their reduced, one-electron form. In order to avoid displaying a large number of the occupied-unoccupied molecular orbital pairs contributing to the operators, we have introduced a natural-orbital representation of the reduced doorway and window operators. In this compact representation, the reduced operators are given as sums over a few particle-hole pairs. The particle (hole) natural orbitals are defined via a unitary transformation among unoccupied (occupied) molecular orbitals that diagonalizes the reduced operator from the left (right). The real-time, real-space evolution of the valence wave packet created in quinolinol by a 600-attosecond pulse was visualized using the snapshots of the natural-orbital pairs for various values of the delay. The dependence of the stimulated Raman signal on the delay can be explained in terms of the real-time, real-space evolution of the pump-induced density matrix wave packet.

ACKNOWLEDGMENT

The support from the Chemical Sciences, Geosciences and Biosciences Division, Office of Basic Energy Sciences, Office of Science, U.S. Department of Energy is gratefully acknowledged.

APPENDIX A: DOORWAY-WINDOW REPRESENTATION OF THE PUMP-PROBE SIGNAL

In the double bracket (Liouville space) notation, $R^{(3)}$ is given by [12]

$$R^{(3)}(t_3,t_2,t_1) = i^3\langle\langle V(t)|\mathcal{G}(t_3)\mathcal{V}\mathcal{G}(t_2)\mathcal{V}\mathcal{G}(t_1)\mathcal{V}|\rho(-\infty)\rangle\rangle. \tag{A1}$$

Given that the delay τ is longer than the pulses's durations, the lower integration limit on t_2 in Eq. (3) can be extended to $-\infty$ since $\mathcal{E}_2(t-t_3-\tau)\mathcal{E}_1(t-t_3-t_2)=0$ unless $t_2 > \tau$. Changing the integration variables t to $t-t_3-\tau$ and t_2 to $t-t_3-t_2$, we recast Eq. (3) into

$$S(\omega_1,\omega_2,\tau) = \mathrm{Im}\int_{-\infty}^{\infty} dt \int_0^{\infty} dt_3 \int_{-\infty}^{\infty} dt_2 \int_0^{\infty} dt_1 R^{(3)}(t_3,t-t_2+\tau,t_1) \times[\mathcal{E}_2^*(t+t_3)\mathcal{E}_2(t)\mathcal{E}_1(t_2)\mathcal{E}_1^*(t_2-t_1)e^{i\omega_2 t_3 - i\omega_1 t_1}$$

$$+\mathcal{E}_2^*(t+t_3)\mathcal{E}_2(t)\mathcal{E}_1^*(t_2)\mathcal{E}_1(t_2-t_1)e^{i\omega_2 t_3+i\omega_1 t_1}]. \quad \text{(A2)}$$

We next define the doorway operator

$$|D(\omega_1,\tau)\rangle\rangle = \mathcal{G}(\tau)\int_{-\infty}^{\infty}dt_2\int_0^{\infty}dt_1\mathcal{E}_1(t_2)\mathcal{E}_1^*(t_2-t_1)e^{-i\omega_1 t_1}\times\mathcal{G}(-t_2)\mathcal{V}\mathcal{G}(t_1)\mathcal{V}|\rho(-\infty)\rangle\rangle + \mathcal{G}(\tau)\int_{-\infty}^{\infty}dt_2\int_0^{\infty}dt_1\mathcal{E}_1^*(t_2)\mathcal{E}_1(t_2-t_1)e^{+i\omega_1 t_1}\times\mathcal{G}(-t_2)\mathcal{V}\mathcal{G}(t_1)\mathcal{V}|\rho(-\infty)\rangle\rangle \quad \text{(A3)}$$

and the window operator

$$\langle\langle W(\omega_2)| = \int_{-\infty}^{\infty}dt\int_0^{\infty}dt_3\mathcal{E}_2^*(t+t_3)\mathcal{E}_2(t)e^{i\omega_2 t_3}\times\langle\langle V|\mathcal{G}(t_3)\mathcal{V}\mathcal{G}(t). \quad \text{(A4)}$$

Equation (A2) can then be recast in the form

$$S(\omega_2,\omega_1,\tau) = \mathrm{Re}\langle\langle W(\omega_2)|D(\omega_1,\tau)\rangle\rangle, \quad \text{(A5)}$$

where we used the property $\mathcal{G}(t-t_2+\tau)=\mathcal{G}(t)\mathcal{G}(\tau)\mathcal{G}^{\dagger}(t_2)$.

Expanding $\mathcal{G}$ in molecular electronic eigenstates [Eq. (5)] gives the sum-over-state expressions for $\hat{D}$ and $\hat{W}$

$$\hat{D} = \sum_{\nu_1,\nu_2}|\nu_1\rangle\langle g_0|V_{\nu_1\nu_2}V_{\nu_2 g_0}\mathcal{I}_1(-\omega_{\nu_1 g_0},\omega_{\nu_2 g_0}-\omega_1) + \sum_{\nu_1,\nu_2}|g_0\rangle\langle\nu_1|V_{\nu_2\nu_1}V_{g_0\nu_2}\mathcal{I}_1(\omega_{\nu_1 g_0},-\omega_{\nu_2 g_0}-\omega_1) - \sum_{\nu_1,\nu_2}|\nu_1\rangle\langle\nu_2|V_{g_0\nu_2}V_{\nu_1 g_0}\mathcal{I}_1(-\omega_{\nu_1\nu_2},\omega_{\nu_1 g_0}-\omega_1) - \sum_{\nu_1,\nu_2}|\nu_2\rangle\langle\nu_1|V_{\nu_2 g_0}V_{g_0\nu_1}\mathcal{I}_1(-\omega_{\nu_2\nu_1},-\omega_{\nu_1 g_0}-\omega_1)+\mathrm{H.c.}, \quad \text{(A6)}$$

$$\hat{W}^{\dagger} = \sum_{\nu_1,\nu_2,\nu_3}|\nu_2\rangle\langle\nu_1|V_{\nu_2\nu_3}V_{\nu_3\nu_1}\mathcal{I}_2(-\omega_{\nu_1\nu_2},\omega_2+\omega_{\nu_1\nu_3}) - \sum_{\nu_1,\nu_2,\nu_3}|\nu_2\rangle\langle\nu_1|V_{\nu_3\nu_1}V_{\nu_2\nu_3}\mathcal{I}_2(-\omega_{\nu_1\nu_2},\omega_2-\omega_{\nu_2\nu_3}), \quad \text{(A7)}$$

where

$$\mathcal{I}_j(\Omega_2,\Omega_1) = \int_{-\infty}^{\infty}dt_2\int_0^{\infty}dt_1\mathcal{E}_j^*(t_2)\mathcal{E}_j(t_2-t_1)e^{i\Omega_2 t_2+i\Omega_1 t_1}. \quad \text{(A8)}$$

$\mathcal{I}(\Omega_2,\Omega_1)$ rapidly decays with increasing Ω_1 and Ω_2 and for a Gaussian pulse with the 600-attosecond FWHM does not exceed 10% of its maximum value for $|\Omega_1|$, $|\Omega_2\pm\Omega_1| \geqslant 6$ eV. Neglecting the contribution of the off-resonant transitions (i.e., $\omega_{e_1 g_0} > \omega_1 + 6$ eV, $\omega_{gg_0} > 12$ eV), Eq. (A6) is recast into

$$\hat{D} = \hat{D}_g + \hat{D}_e, \quad \text{(A9)}$$

$$\hat{D}_g = \sum_{g,e_1}|g\rangle\langle g_0|V_{ge_1}V_{e_1 g_0}\mathcal{I}_1(\omega_{gg_0},\omega_1-\omega_{e_1 g_0})+\mathrm{H.c.}, \quad \text{(A10)}$$

$$\hat{D}_e = \sum_{e_1,e_1'}|e_1\rangle\langle e_1'|V_{g_0 e_1'}V_{e_1 g_0}\mathcal{I}_1(\omega_{e_1 e_1'},\omega_1-\omega_{e_1 g_0})-\mathrm{H.c.} \quad \text{(A11)}$$

Similarly, Eq. (A7) is recast into

$$\hat{W} = \hat{W}_g + \hat{W}_e, \quad \text{(A12)}$$

$$\hat{W}_g = \sum_{g,g',e_2}|g'\rangle\langle g|V_{g' e_2}V_{e_2 g}\mathcal{I}_2(-\omega_{gg'},\omega_2-\omega_{e_2 g}), \quad \text{(A13)}$$

$$\hat{W}_e = \sum_{f,e_2,e_2'}|e_2'\rangle\langle e_2|V_{e_2' f}V_{f e_2}\mathcal{I}_2(-\omega_{e_1 e_1'},\omega_2-\omega_{f e_2}) - \sum_{g,e_2,e_2'}|e_2'\rangle\langle e_2|V_{g e_2}V_{e_2' g}\mathcal{I}_2(-\omega_{e_1 e_1'},\omega_2-\omega_{e_2' g}). \quad \text{(A14)}$$

APPENDIX B: NATURAL-ORBITAL REPRESENTATION OF THE DOORWAY AND WINDOW OPERATORS

The doorway and the window natural orbitals are defined by analogy with the natural transition orbitals introduced in Ref. [17]. For the doorway operator we define a $N_o\times N_v$ (N_v being the number of unoccupied orbitals) matrix $\mathbf{D}(\tau)$ such that $D_{ia}(\tau)=d_{ia}e^{-i(\epsilon_a-\epsilon_i)\tau}$ [cf. Eq. (23)]. The doorway hole and particle natural orbitals are defined by unitary transformations among the occupied and unoccupied molecular orbitals, respectively,

$$(\phi_1^h,\phi_2^h,\ldots,\phi_{N_o}^h) = (\phi_1,\phi_2,\ldots,\phi_{N_o})\mathbf{U}^{hh}, \quad \text{(B1)}$$

$$(\phi_1^p,\phi_2^p,\ldots,\phi_{N_v}^p) = (\phi_{N_o+1},\phi_2,\ldots,\phi_{N_o+N_v})\mathbf{U}^{pp}. \quad \text{(B2)}$$

The $N_o\times N_o$ matrix $\mathbf{U}^{hh}\equiv(\mathbf{u}_1^h,\mathbf{u}_2^h,..,\mathbf{u}_{N_o}^h)$ and the $N_v\times N_v$ matrix $\mathbf{U}^{pp}\equiv(\mathbf{u}_1^p,\mathbf{u}_2^p,..,\mathbf{u}_{N_v}^p)$ are determined by solving the eigenvalue equations

$$\mathbf{D}\mathbf{D}^{\dagger}\mathbf{u}_i^h = \lambda_i^h \mathbf{u}_i^h, i = 1, \ldots, N_o, \tag{B3}$$

$$\mathbf{D}^{\dagger}\mathbf{D}\mathbf{u}_i^p = \lambda_i^p \mathbf{u}_i^p, i = 1, \ldots, N_v, \tag{B4}$$

so that

$$\left|(\mathbf{U}^{hh})^{\dagger}\mathbf{D}\mathbf{U}^{pp}\right| = \mathrm{diag}\sqrt{\lambda_i^p}. \tag{B5}$$

Correspondingly, in terms of ϕ^h, ϕ^p the reduced doorway operator [Eq. (23)] is given by

$$D_v(\boldsymbol{r},\boldsymbol{r}',\tau) = \sum_{\xi} d_{\xi}(\tau)\phi_{\xi}^p(\boldsymbol{r},\tau)\phi_{\xi}^{h*}(\boldsymbol{r}',\tau) + \mathrm{H.c.} \tag{B6}$$

[1] J. Stohr, *NEXAFS Spectroscopy* (Springer, New York, 1996).
[2] I. V. Tomov, D. A. Oulianov, P. L. Chen, and P. M. Rentzepis, J. Phys. Chem. B **103**, 7081 (1999).
[3] L. X. Chen, W. J. H. Jager, G. Jennings, D. J. Gosztola, A. Munkholm, and J. P. Hessler, Science **292**, 262 (2001).
[4] M. Saes, C. Bressler, R. Abela, D. Grolimund, S. L. Johnson, P. A. Heimann, and M. Chergui, Phys. Rev. Lett. **90**, 047403 (2003).
[5] M. Hentschel, R. Kienberger, C. Spielmann, G. A. Reider, N. Milosevic, T. Brabec, P. Corkum, U. Heinzmann, M. Drescher, and F. Krausz, Nature (London) **414**, 509 (2001).
[6] M. Drescher, M. Hentschel, R. Kienberger, M. Uiberacker, V. Yakovlev, A. Scrinizi, T. Westerwalbesloh, U. Kleineberg, U. Heinzmann, and F. Krausz, Nature (London) **419**, 803 (2002).
[7] C. Bressler and M. Chergui, Chem. Rev. (Washington, D.C.) **104**, 1781 (2004).
[8] V. Felicissimo, F. Guimaraes, F. Gel'mukhanov, A. Cesar, and H. Agren, J. Chem. Phys. **122**, 094319 (2005).
[9] S. Tanaka and S. Mukamel, J. Electron Spectrosc. Relat. Phenom. **136**, 185 (2004).
[10] S. Tanaka and S. Mukamel, Phys. Rev. Lett. **89**, 043001 (2002).
[11] S. Mukamel, Phys. Rev. B **72**, 235110 (2005).
[12] S. Mukamel, *Principles of Nonlinear Optical Spectroscopy* (Oxford University Press, New York, 1995).
[13] Y. J. Yan and S. Mukamel, Phys. Rev. A **41**, 6485 (1990).
[14] W. H. E. Schwarz and R. J. Buenker, Chem. Phys. **13**, 153 (1976).
[15] I. V. Schweigert and S. Mukamel (unpublished).
[16] P.-O. Löwdin, Phys. Rev. **97**, 1474 (1955).
[17] R. L. Martin, J. Chem. Phys. **118**, 4775 (2003).
[18] A. D. Becke, J. Chem. Phys. **98**, 5648 (1993).
[19] W. J. Hehre, R. Ditchfield, and J. A. Pople, J. Chem. Phys. **56**, 2257 (1972).
[20] C. Hannay, D. Duflot, J. Flament, and M. Hubin-Franskin, J. Chem. Phys. **110**, 5600 (1999).
[21] J. T. Francis and A. P. Hitchcock, J. Phys. Chem. **96**, 6598 (1992).